Hindawi Publishing Corporation
Journal of Robotics
Volume 2014, Article ID 967251, 10 pages
http://dx.doi.org/10.1155/2014/967251

Research Article

Kinematics, Singularity, and Workspaces of a Planar 4-Bar Tensegrity Mechanism

Zhifei Ji, Tuanjie Li, and Min Lin

School of Electro-Mechanical Engineering, Xidian University, P.O. Box 188, Xi'an 710071, China

Correspondence should be addressed to Zhifei Ji; zfji18@163.com

Received 21 December 2013; Revised 20 February 2014; Accepted 20 February 2014; Published 25 March 2014

Academic Editor: Gordon R. Pennock

Compared with conventional mechanisms, tensegrity mechanisms have many attractive characteristics such as light weight, high ratio of strength to weight, and accuracy of modeling. In this paper, the kinematics, singularity, and workspaces of a planar 4-bar tensegrity mechanism have been investigated. Firstly, the analytical solutions to the forward and inverse kinematic problems are found by using an energy based method. Secondly, the definition of a tensegrity mechanism's Jacobian is introduced. As a consequence, the singularity analysis of the planar 4-bar tensegrity mechanism has been completed. Thirdly, the actuator and output workspaces are mapped. Finally, some attractive characteristics of the mechanism are concluded.

1. Introduction

As the complexity of robotic applications in space increases, new demands for lighter and quicker mechanisms arise. Tensegrity mechanisms can be viewed as one alternative solution to conventional mechanisms. For this reason, a planar 4-bar tensegrity mechanism is proposed in this paper and the kinematics and statics of the mechanism are studied.

The term tensegrity was created by Fuller [1] as a combination of the words tensional and integrity. It seems that he was inspired by some novel sculptures completed by Snelson [2]. The detailed history of tensegrity systems was reviewed by Motro [3]. Tensegrity systems are formed by a set of compressive components and tensile components. Tensegrity systems have advantages of light weight, deployability, being easily tunable, and so forth. Due to these attractive characteristics, tensegrity systems have been used in several disciplines such as architecture, biology, aerospace, mechanics, and robotics during the last fifty years [4].

The applications of tensegrity systems can be divided into two main branches. One application is used as structures and the other one is used as mechanisms. In addition, the research of tensegrity structures has two main issues, which are the form-finding problem and the behaviors under external loads. The form finding of a tensegrity structure corresponds to the computation of the structure's equilibrium shape for a given set of parameters. This problem has been studied by many authors [5–7]. Moreover, a review of form-finding methods is given by Tibert and Pellegrino [5]. The behaviors of tensegrity structures under external loads have also been researched by many researchers [8, 9]. A static analysis of tensegrity structures was given by Juan and Mirats Tur [10]. When some components (rigid rods or springs) are actuated, tensegrity mechanisms can be obtained. In the past twenty years, several tensegrity mechanisms have been proposed [11–17]. The proposed applications of tensegrity mechanisms range from a flight simulator [18], a space telescope [19], and a robot [20] to a sensor [21]. For tensegrity mechanisms, the dynamics and open problems have been reviewed by Mirats Tur and Juan [22].

During the past twenty years, considerable research has been performed on the control, statics, and dynamics of class-1 tensegrity mechanisms. However, there are few articles relating to class-2 tensegrity mechanisms, especially on the study of them. The main objective of this paper is to perform an analytical investigation of the kinematics, singularity, and workspaces of a planar 4-bar (class-2) tensegrity mechanism. The definitions of class-1 and class-2 tensegrity systems are given by Skelton and Oliveira [4].

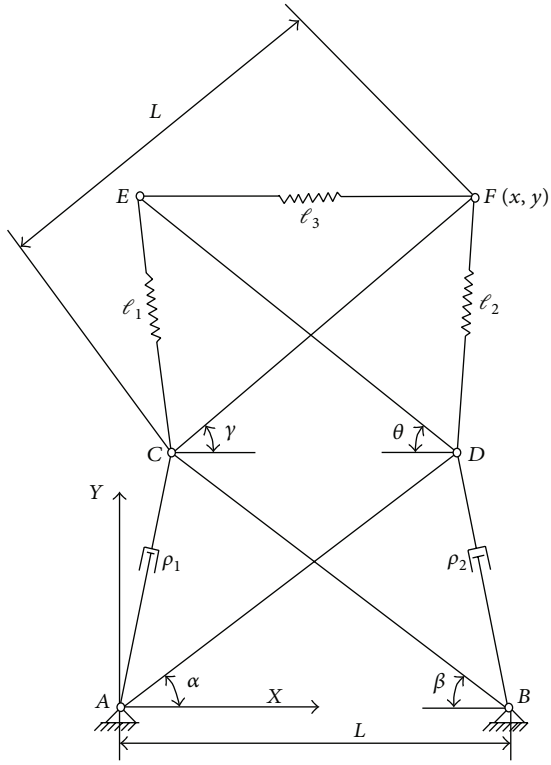

Figure 1: Planar 4-bar tensegrity mechanism.

Marc Arsenault and Gosselin [23] introduced the conditions of static balancing of tensegrity mechanisms, which leads to important simplifications in the analysis of tensegrity mechanisms. These conditions of the static balancing of tensegrity mechanism were used in this paper to find the analytical solutions to the forward and inverse kinematic problems of the planar 4-bar tensegrity mechanism.

This paper is organized as follows. In Section 2, the planar 4-bar tensegrity mechanism was introduced. The forward and inverse kinematic analysis was performed in Section 3. Furthermore, the Jacobian was computed and the singularity configurations were obtained in Section 4. The actuator and output workspaces were mapped, respectively, in Section 5. Finally, conclusions were reported in Section 6.

2. Mechanism Description

A diagram of the planar 4-bar tensegrity mechanism considered here is shown in Figure 1. It is composed of three springs, four bars, and two prismatic actuators. The bars of length L are joining node pairs DE, CF, BC, and AD while the springs are joining node pairs CE, EF, and DF. Moreover, the prismatic actuators are used to vary the distances between node pairs AC and BD.

As shown in Figure 1, the bars, springs, and prismatic actuators are connected to each other at each node by 2D frictionless rotational joints. Furthermore, nodes A and B are fixed to the ground and the whole mechanism lies in a horizontal plane. From Figure 1, it can be seen that joints A and B have restrained translational DOF in x- and y-axes but free rotational DOF. In addition, the angle between the x-axis and the bar joining nodes AD is defined as α while the angle between the horizontal and the bar joining nodes BC is defined as β. Moreover, the angle between the x-axis and the bar joining nodes CF is defined as γ while the angle between the horizontal and the bar joining nodes DE is defined as θ. From Figure 1, it can also be observed that the distance between nodes A and B is L.

In Figure 1, the stiffness of the springs of lengths ℓ_i ($i = 1, 2, 3$) is denoted by K. Furthermore, it is assumed that the springs have zero free length. This hypothesis is not problematic since, as was explained by Gosselin [24] and Shekarforoush et al. [25], virtual zero-free-length spring can be created by extending the actual spring beyond its attachment point. The actuator lengths (ρ_1 and ρ_2) are chosen as the mechanism's input variables while the Cartesian coordinates of node F (x and y) are chosen as the mechanism's output variables. From Figure 1, it can be seen that the shape of the mechanism can be determined for the given actuator lengths. Moreover, the Y coordinates of nodes C and D are chosen to be nonnegative. For this reason, the ranges imposed to α and β can be obtained as follows:

$$0 \leq \alpha \leq \pi, \qquad 0 \leq \beta \leq \pi. \tag{1}$$

Furthermore, the ranges imposed to θ and γ are chosen as

$$0 < \gamma < \pi, \qquad 0 < \theta < \pi. \tag{2}$$

From Figure 1, it can be observed that the mechanism is unstable in the case of DE and CF being parallel. In particular, in this case, the mechanism cannot be in equilibrium. For this reason, $\gamma + \theta \neq \pi$.

3. Kinematic and Static Analysis

For a tensegrity mechanism, the kinematics and statics should be considered simultaneously since the relationships between the input and output variables depend not only on the mechanism's geometry but also on the internal forces in the springs. For this reason, it is always assumed that the planar 4-bar tensegrity mechanism is in equilibrium. Under this assumption, the explicit relationships between the input and output variables can be developed.

3.1. Forward Kinematic Analysis. For the mechanism considered here, the forward kinematic analysis consists in computing the Cartesian coordinates of node F for the given actuator lengths. From Figure 1, it can be seen that when the actuator lengths (ρ_1 and ρ_2) are specified, the triangle formed by nodes A, B, and D and the triangle formed by nodes A, B, and C are determined. As a consequence, the movement of node E is confined to a rotation centered on node D. Moreover, the movement of node F is also constrained to a rotation centered on node C. For the mechanism shown in Figure 1, the potential energy of the system will reach its minimum when the mechanism is in equilibrium. Therefore, the relationships between the input and output variables can be obtained by minimizing the potential energy with respect to a set of parameters, chosen here as θ and γ.

From Figure 1, the coordinates of nodes A, B, C, and D can be obtained as follows:

$$\mathbf{P}_A = \begin{bmatrix} 0 \\ 0 \end{bmatrix}, \qquad \mathbf{P}_B = \begin{bmatrix} L \\ 0 \end{bmatrix}, \\ \mathbf{P}_C = \begin{bmatrix} L(1-\cos\beta) \\ L\sin\beta \end{bmatrix}, \qquad \mathbf{P}_D = \begin{bmatrix} L\cos\alpha \\ L\sin\alpha \end{bmatrix}. \tag{3}$$

With the coordinates of nodes C and D now known, the coordinates of nodes E and F can be written in the following form:

$$\mathbf{P}_E = \begin{bmatrix} L(\cos\alpha - \cos\theta) \\ L(\sin\alpha + \sin\theta) \end{bmatrix}, \\ \mathbf{P}_F = \begin{bmatrix} L(1 - \cos\beta + \cos\gamma) \\ L(\sin\beta + \sin\gamma) \end{bmatrix}. \tag{4}$$

Since the Cartesian coordinates of node F are chosen as the output variables, we therefore write

$$x = L(1 - \cos\beta + \cos\gamma), \\ y = L(\sin\beta + \sin\gamma). \tag{5}$$

Furthermore, the lengths of the springs CE, EF, and FD can be easily calculated according to (3) and (4). Then, the potential energy of the mechanism takes the form

$$\begin{aligned} U &= \sum_{i=1}^{3} \frac{1}{2} K \ell_i^2 \\ &= \frac{KL^2}{2} [13 + 6(\cos\alpha\cos\beta - \sin\alpha\sin\beta - \cos\alpha - \cos\beta) \\ &\quad + 4(1 - \cos\beta - \cos\alpha) \\ &\quad \cdot (\cos\gamma + \cos\theta) + 2\cos(\theta + \gamma) \\ &\quad + (\sin\alpha - \sin\beta)(\sin\theta - \sin\gamma)]. \end{aligned} \tag{6}$$

As shown in Figure 1, a cosine law for the triangle formed by nodes A, B, and D can be written as

$$\cos\alpha = \frac{2L^2 - \rho_2^2}{2L^2}. \tag{7}$$

Moreover, a cosine law for the triangle formed by nodes A, B, and C can be written as

$$\cos\beta = \frac{2L^2 - \rho_1^2}{2L^2}. \tag{8}$$

Due to the ranges imposed to α and β, the expressions for $\sin\alpha$ and $\sin\beta$ can be derived as follows:

$$\sin\alpha = \sqrt{1 - \cos^2\alpha} = \frac{\rho_2\sqrt{4L^2 - \rho_2^2}}{2L^2}, \tag{9}$$

$$\sin\beta = \sqrt{1 - \cos^2\beta} = \frac{\rho_1\sqrt{4L^2 - \rho_1^2}}{2L^2}. \tag{10}$$

Substituting (7), (8), (9), and (10) into (6), the potential energy of the mechanism can be expressed as

$$\begin{aligned} U = \frac{KL^2}{2} \Bigg[& \frac{3}{2L^4} \left(\rho_1^2\rho_2^2 - \prod_{i=1}^{2} \rho_i \sqrt{4L^2 - \rho_i^2} \right) + 7 \\ & + \frac{2}{L^2} \left(\rho_1^2 + \rho_2^2 - 2L^2 \right) (\cos\gamma + \cos\theta) \\ & + \frac{2}{L^2} \left(\rho_2\sqrt{4L^2 - \rho_2^2} - \rho_1\sqrt{4L^2 - \rho_1^2} \right) \\ & \times (\sin\theta - \sin\gamma) + 2\cos(\theta + \gamma) \Bigg]. \end{aligned} \tag{11}$$

By differentiating U with respect to θ and γ separately and equating the results to zero, the following equations are generated:

$$\begin{aligned} \frac{\partial U}{\partial \theta} = \frac{KL^2}{2} \Bigg[& \frac{2}{L^2} \left(\rho_1^2 + \rho_2^2 - 2L^2 \right) (-\sin\theta) + \frac{2}{L^2} \\ & \times \left(\rho_2\sqrt{4L^2 - \rho_2^2} - \rho_1\sqrt{4L^2 - \rho_1^2} \right) \\ & \times \cos\theta - 2\sin(\theta + \gamma) \Bigg] = 0, \end{aligned} \tag{12}$$

$$\begin{aligned} \frac{\partial U}{\partial \gamma} = \frac{KL^2}{2} \Bigg[& \frac{2}{L^2} \left(\rho_1^2 + \rho_2^2 - 2L^2 \right) (-\sin\gamma) - \frac{2}{L^2} \\ & \times \left(\rho_2\sqrt{4L^2 - \rho_2^2} - \rho_1\sqrt{4L^2 - \rho_1^2} \right) \\ & \times (\cos\gamma) - 2\sin(\theta + \gamma) \Bigg] = 0. \end{aligned} \tag{13}$$

Due to $\gamma + \theta \neq \pi$, the following equation can be obtained by eliminating the expression $\sin(\theta + \gamma)$ from (12) and (13):

$$\begin{aligned} \theta = \gamma + 2\tan^{-1} & \\ & \times \left[\frac{\left(\rho_2\sqrt{4L^2 - \rho_2^2} - \rho_1\sqrt{4L^2 - \rho_1^2} \right)}{\left(\rho_1^2 + \rho_2^2 - 2L^2 \right)} \right]. \end{aligned} \tag{14}$$

Substituting (14) into (13) yields

$$\begin{aligned} & \left[-N_1 \left(N_0^2 + N_1^2 \right) - 3N_0N_1 \right] t_1^4 \\ & + 2 \left[N_0 \left(N_0^2 + N_1^2 \right) - \left(N_0^2 - N_1^2 \right) \right] t_1^3 \\ & - 2N_0N_1t_1^2 + 2 \left[N_0 \left(N_0^2 + N_1^2 \right) + \left(N_0^2 - N_1^2 \right) \right] t_1 \\ & + N_1 \left(N_0^2 + N_1^2 \right) + N_0N_1 = 0, \end{aligned} \tag{15}$$

where $t_1 = \tan(\gamma/2)$. The expressions for N_0 and N_1 are detailed in Appendix A. It is apparent that (15) is an equation of degree 4 in t_1. Solving (15) for t_1, we obtain

$$\begin{aligned} t_{1j} = {} & \frac{1}{4}\left[(-1)^{j+1}\left(E_1^2 - E_2 + E_5\right)^{1/2} - E_1\right] + \frac{\delta_1}{4} \\ & \times \left[\left(E_1 + (-1)^j\left(E_1^2 - E_2 + E_5\right)^{1/2}\right.\right. \\ & \left. -8\left(E_1E_5 - 2M_3\right)(-1)^j\right) \\ & \left.\times\left(\left(E_1^2 - E_2 + E_5\right)^{1/2} - 8E_5\right)^{-1}\right]^{1/2}, \end{aligned} \tag{16}$$

where $\delta_1 = \pm 1$. Moreover, the variables E_ξ ($\xi = 1, \ldots, 5$) are also detailed in Appendix A. t_{1j} represents four solutions to (15) for $j = 1, 2$. Computing the arctangent of t_1 generates a unique solution for γ due to the range imposed to γ. Moreover, negative solutions for t_1 should be eliminated. With the solutions for γ now known, the solutions to the forward kinematic problem can be found by substituting (8) and (10) into (5).

3.2. Inverse Kinematic Analysis. The inverse kinematic analysis of the mechanism corresponds to the computation of the actuator lengths for the given Cartesian coordinates of node F.

Eliminating the parameter, γ, from (5) yields

$$\begin{aligned} & \left[(x-L)^2 + y^2 - 2L(x-L)\right]t_2^2 \\ & \quad - 4yLt_2 + (x-L)^2 + y^2 + 2L(x-L) = 0, \end{aligned} \tag{17}$$

where $t_2 = \tan(\beta/2)$.

Solving (17) for t_2, we obtain

$$\begin{aligned} t_2 = {} & \left(2yL \pm \left\{4y^2L^2 - \left[(x-L)^2 + y^2 - 2L(x-L)\right]\right.\right. \\ & \left.\left.\times\left[(x-L)^2 + y^2 + 2L(x-L)\right]\right\}^{1/2}\right) \\ & \times\left((x-L)^2 + y^2 - 2L(x-L)\right)^{-1}. \end{aligned} \tag{18}$$

Substituting the expression $t_2 = \tan(\beta/2)$ into (8) yields

$$\rho_1 = \frac{2Lt_2}{\sqrt{1+t_2^2}}. \tag{19}$$

Therefore, substituting (18) into (19), two solutions for ρ_1 are found. In the following paragraphs, we will find the solutions for ρ_2.

By substituting (8) and (10) into (5), we obtain

$$\begin{aligned} \sin\gamma &= \frac{2Ly - \rho_1\sqrt{4L^2 - \rho_1^2}}{2L^2}, \\ \cos\gamma &= \frac{2Lx - \rho_1^2}{2L^2}. \end{aligned} \tag{20}$$

Moreover, substituting (7), (8), (9), and (10) into (14) yields

$$\theta = \gamma + 2\tan^{-1}\left[\frac{\left(2L^2\sin\alpha - \rho_1\sqrt{4L^2 - \rho_1^2}\right)}{\left(\rho_1^2 - 2L^2\cos\alpha\right)}\right]. \tag{21}$$

Substituting (20) and (21) into (13) and rearranging yields

$$\lambda_1 t_3^4 + \lambda_2 t_3^3 + \lambda_3 t_3^2 + \lambda_4 t_3 + \lambda_5 = 0, \tag{22}$$

where $t_3 = \tan(\alpha/2)$. The expressions for λ_ζ ($\zeta = 1, \ldots, 5$) are detailed in Appendix B.

It can be seen that (22) is an equation of degree 4 in t_3. Therefore, solving (22), the following is obtained:

$$\begin{aligned} t_{3\mu} = {} & \frac{(-1)^{\mu+1}\left(4\lambda_1^2\eta - 4\lambda_1\lambda_3 + \lambda_2^2\right)^{1/2} - \lambda_2}{2\lambda_1} \\ & + \frac{\delta_2}{2}\left\{\frac{1}{4\lambda_1^2}\left[\lambda_2 + (-1)^\mu\left(4\lambda_1^2\varphi - 4\lambda_1\lambda_3 + \lambda_2^2\right)^{-1/2}\right]^2\right. \\ & - (-1)^\mu 2\left(\lambda_2\eta - 2\lambda_4\right) \\ & \left.\times\left(4\lambda_1^2\varphi - 4\lambda_1\lambda_3 + \lambda_2^2\right)^{-1/2} - 2\eta\right\}^{1/2}, \end{aligned} \tag{23}$$

where

$$\begin{aligned} \eta = {} & \frac{\lambda_3}{3\lambda_1} + \left[\frac{-Q}{2} + \sqrt{\frac{Q^2}{4} - \frac{P^3}{27}}\right]^{1/3} \\ & + \left[\frac{-Q}{2} - \sqrt{\frac{Q^2}{4} - \frac{P^3}{27}}\right]^{1/3}, \end{aligned} \tag{24}$$

and where

$$\begin{aligned} P &= \frac{1}{\lambda_1^2}\left[\lambda_2\lambda_4 - 4\lambda_1\lambda_5 - \frac{1}{3}\lambda_3^2\right], \\ Q &= \frac{1}{\lambda_1^3}\left[\frac{2\lambda_3^3}{27} + \frac{\lambda_3}{3}\left(\lambda_2\lambda_4 - 4\lambda_1\lambda_5\right)\right. \\ & \left. + \left(4\lambda_1\lambda_3\lambda_5 - \lambda_2^2\lambda_5 - \lambda_1\lambda_4^2\right)\right]. \end{aligned} \tag{25}$$

Substituting the expression $t_3 = \tan(\alpha/2)$ into (7), we obtain

$$\rho_2 = \frac{2Lt_3}{\sqrt{1+t_3^2}}. \tag{26}$$

In (23), it should be noted that $\delta_2 = \pm 1$. Moreover, $t_{3\mu}$ represents four solutions to (22) for $\mu = 1, 2$. Considering the range imposed to α, negative solutions for t_3 should be eliminated. Substituting (23) into (26), the solutions for ρ_2 are found.

Two solutions for ρ_1 are given by (19). Four solutions for ρ_2 can be found by (26). In particular, if these solutions for ρ_1 and ρ_2 are all nonnegative, eight solutions to the inverse kinematic problem are found.

4. Singularity Analysis

The singularity analysis of a mechanism can be completed by analyzing its Jacobian. The objective of this section is to obtain singular configurations of the planar 4-bar tensegrity mechanism.

4.1. Mechanism Jacobian. For conventional mechanisms, Jacobian is used to describe the relations between input and output velocities. However, for tensegrity mechanisms, these relationships cannot be established since there are more degrees of freedom than actuators. When a tensegrity mechanism is in equilibrium, its Jacobian can be defined as

$$\delta\boldsymbol{\varphi} = \mathbf{J}\delta\boldsymbol{\psi}, \tag{27}$$

where $\boldsymbol{\varphi} = [x, y]^{\mathrm{T}}$ and $\boldsymbol{\psi} = [\rho_1, \rho_2]^{\mathrm{T}}$. For the 4-bar tensegrity mechanism considered here, $\mathbf{J}$ can be written as follows:

$$\mathbf{J} = \begin{bmatrix} \dfrac{\partial x}{\partial \rho_1} & \dfrac{\partial x}{\partial \rho_2} \\ \dfrac{\partial y}{\partial \rho_1} & \dfrac{\partial y}{\partial \rho_2} \end{bmatrix}. \tag{28}$$

Substituting (8) and (10) into (5), we obtain

$$\begin{aligned} x &= \frac{\rho_1^2}{2L} + L\cos\gamma, \\ y &= \frac{\rho_1}{2L}\sqrt{4L^2 - \rho_1^2} + L\sin\gamma. \end{aligned} \tag{29}$$

The elements of the Jacobian matrix, $\mathbf{J}$, can be computed as follows:

$$\begin{aligned} \frac{\partial x}{\partial \rho_1} &= \frac{\rho_1}{L} - L\sin\gamma\frac{\partial \gamma}{\partial \rho_1}, \\ \frac{\partial x}{\partial \rho_2} &= -L\sin\gamma\frac{\partial \gamma}{\partial \rho_2}, \\ \frac{\partial y}{\partial \rho_1} &= \frac{2L^2 - \rho_1^2}{L\sqrt{4L^2 - \rho_1^2}} + L\cos\gamma\frac{\partial \gamma}{\partial \rho_1}, \\ \frac{\partial y}{\partial \rho_2} &= L\cos\gamma\frac{\partial \gamma}{\partial \rho_2}. \end{aligned} \tag{30}$$

Then, in the following paragraphs, we will derive the expression for $\partial\gamma/\partial\rho_i$ for $i = 1, 2$. Substituting (7), (8), (9), and (10) into (12) and (13) yields

$$\begin{aligned} &2(1 - \cos\alpha - \cos\beta)\sin\theta - 2(\sin\alpha - \sin\beta)\cos\theta \\ &\quad + \sin(\theta + \gamma) = 0, \\ &2(1 - \cos\alpha - \cos\beta)(-\sin\gamma) \\ &\quad - 2(\sin\alpha - \sin\beta)\cos\gamma - \sin(\theta + \gamma) = 0. \end{aligned} \tag{31}$$

By differentiating both sides of (31) and with respect to ρ_i, for $i = 1, 2$, we obtain

$$\begin{aligned} &[2\cos\theta + \cos(\theta + \gamma) - 2\cos(\beta - \theta) - 2\cos(\alpha - \theta)]\frac{\partial \theta}{\partial \rho_i} \\ &\quad + \cos(\theta + \gamma)\frac{\partial \gamma}{\partial \rho_i} - 2\cos(\alpha + \theta)\frac{\partial \alpha}{\partial \rho_i} \\ &\quad + 2\cos(\beta - \theta)\frac{\partial \beta}{\partial \rho_i} = 0, \end{aligned} \tag{32}$$

$$\begin{aligned} &[2\cos(\beta + \gamma) + 2\cos(\alpha - \gamma) - \cos(\theta + \gamma) - 2\cos\gamma]\frac{\partial \gamma}{\partial \rho_i} \\ &\quad - \cos(\theta + \gamma)\frac{\partial \theta}{\partial \rho_i} - 2\cos(\alpha - \gamma)\frac{\partial \alpha}{\partial \rho_i} \\ &\quad + 2\cos(\beta + \gamma)\frac{\partial \beta}{\partial \rho_i} = 0. \end{aligned} \tag{33}$$

Furthermore, the following equations can be derived from (7) and (8):

$$\frac{\partial \alpha}{\partial \rho_1} = 0, \qquad \frac{\partial \beta}{\partial \rho_2} = 0. \tag{34}$$

Considering the condition shown in (34) and combining (32) with (33), we have

$$\frac{\partial \gamma}{\partial \rho_1} = \frac{\Phi_1}{\Phi_2}\cdot\frac{\partial \beta}{\partial \rho_1}, \tag{35}$$

$$\frac{\partial \gamma}{\partial \rho_2} = \frac{\Phi_3}{\Phi_2}\cdot\frac{\partial \alpha}{\partial \rho_2}, \tag{36}$$

where

$$\begin{aligned} \Phi_1 &= -\{2\cos(\beta - \theta)\cos(\theta + \gamma) + 2\cos(\beta + \gamma) \\ &\quad \times [2\cos\theta - 2\cos(\beta - \theta) \\ &\quad + \cos(\theta + \gamma) - 2\cos(\alpha - \theta)]\}, \\ \Phi_2 &= \cos^2(\theta + \gamma) \\ &\quad + [2\cos\theta + \cos(\theta + \gamma) - 2\cos(\beta - \theta) - 2\cos(\alpha - \theta)] \\ &\quad \cdot [2\cos(\beta + \gamma) + 2\cos(\alpha - \gamma) - \cos(\theta + \gamma) - 2\cos\gamma], \\ \Phi_3 &= 2\cos(\alpha + \theta)\cos(\theta + \gamma) \\ &\quad + 2\cos(\alpha - \gamma)[2\cos\theta + \cos(\theta + \gamma) \\ &\quad - 2\cos(\beta - \theta) - 2\cos(\alpha - \theta)]. \end{aligned} \tag{37}$$

Moreover, the expressions for $\partial\alpha/\partial\rho_2$ and $\partial\beta/\partial\rho_1$ can be computed from (7) and (8) as follows:

$$\frac{\partial\alpha}{\partial\rho_2} = \frac{-1}{\sqrt{1-\cos^2\alpha}} \cdot \frac{\partial\cos\alpha}{\partial\rho_2} = \frac{2}{\sqrt{4L^2-\rho_2^2}},$$
$$\frac{\partial\beta}{\partial\rho_1} = \frac{-1}{\sqrt{1-\cos^2\beta}} \cdot \frac{\partial\cos\beta}{\partial\rho_1} = \frac{2}{\sqrt{4L^2-\rho_1^2}}. \quad (38)$$

By substituting (35) and (36) into (30), the elements of the mechanism's Jacobian can be computed.

The Jacobian, **J**, describes the relationships between the infinitesimal movements of the actuators and the end-effector (node F) of the mechanism. In addition, the detailed discussion of the Jacobian will be presented in Section 4.2.

4.2. Singular Configurations. The singular configurations of a mechanism correspond to situations where the determinant of **J** is zero, goes to infinity, or is indeterminate.

The determinant of **J** can be derived from (28) as follows:

$$\det(\mathbf{J}) = L^2 \sin(\beta+\gamma) \frac{\partial\beta}{\partial\rho_1} \cdot \frac{\partial\gamma}{\partial\rho_2}. \quad (39)$$

Substituting (36) and (38) into (39), we obtain

$$\det(\mathbf{J}) = \frac{4L^2\sin(\beta+\gamma)}{\sqrt{(4L^2-\rho_1^2)(4L^2-\rho_2^2)}} \cdot \frac{\Phi_3}{\Phi_2}, \quad (40)$$

where the expressions for Φ_2 and Φ_3 are shown in (37). Furthermore, the singular configurations can be obtained by examining (37) and (40). The expressions of these singular configurations and the corresponding behaviors of the mechanism are described as follows.

(i) $\rho_1 = 0$. One has the following.

(1) Node A is coincident with node C.
(2) Finite movements of node F in a direction perpendicular to the line joining nodes C and F are possible while finite movements of node E in a direction perpendicular to the line joining nodes D and E are also possible with actuators being locked.
(3) Infinitesimal movements of node F along a direction parallel to the line joining nodes C and F cannot be generated. Moreover, infinitesimal movements of node E in a direction parallel to the line that joins nodes D and E cannot be generated either with actuators being locked.
(4) External forces applied in a direction perpendicular to the line joining nodes E and D cannot be resisted by the actuators.

(ii) $\rho_2 = 0$. One has the following.

(1) Node B is coincident with node D.
(2) Finite movements of node E along a direction perpendicular to the line joining nodes D and E are possible with actuators being locked.
(3) Infinitesimal movements of node E in a direction parallel to the line that joins nodes D and E cannot be generated with actuators being locked.
(4) External forces applied along a direction perpendicular to the line joining nodes C and F cannot be resisted by the actuators.

(iii) $\rho_1 = 2L$. One has the following.

(1) Node C is located on the x-axis.
(2) Finite movements of Node F along a direction perpendicular to the line joining nodes C and F are possible with actuators locked. Moreover, finite movements of node C in a direction parallel to the y-axis are also possible with actuators being locked.
(3) Infinitesimal movements of node C along a line parallel to the x-axis cannot be generated.
(4) External forces applied in a direction perpendicular to the line joining nodes D and E cannot be resisted by the actuators.

(iv) $\rho_2 = 2L$. One has the following.

(1) Node D is located on the x-axis.
(2) Finite movements of node E along a direction perpendicular to the line joining nodes D and E are possible while finite movements of node D in a direction parallel to the y-axis are also possible with actuators being locked.
(3) Infinitesimal movements of node D along a line parallel to the x-axis cannot be generated.
(4) External forces applied in a direction perpendicular to the line joining nodes C and F cannot be resisted by the actuators.

(v) $\rho_1 = \rho_2 = 2L$. One has the following.

(1) All the nodes of the mechanism are located on the x-axis.
(2) Node F is coincident with node A while node E is coincident with node B.
(3) Finite movements of nodes C,D, E, and F along a direction parallel to the y-axis are possible.
(4) External forces applied in a direction parallel to the y-axis cannot be resisted by the actuators. Moreover, external forces applied along a direction parallel to the x-axis are resisted by the mechanism with no forces generated in the actuators.

(vi) $\rho_1 = \rho_2 = L$. One has the following.

(1) Node C is coincident with node D while node E is coincident with node F.

(2) Finite movements of node E in a direction perpendicular to the line joining nodes D and E are possible. Moreover, the compressive element joining node pairs E and D can gain an arbitrary rotation with respect to node D with actuators being locked.

(3) Infinitesimal movements of node E in a direction parallel to the line joining nodes $D$and E cannot be generated.

(4) External forces applied along a direction perpendicular to the line joining nodes D and E cannot be resisted by the actuators.

(vii) $\sin(\beta + \gamma) = 0$, $\Phi_2 = 0$ and $\Phi_3 = 0$. One has the following.

(1) Finite movements of node E in a direction perpendicular to the line joining nodes D and E are possible while finite movements of node F in a direction perpendicular to the line joining nodes C and F are also possible with actuators being locked.

It can be noted that the mechanism will reach its dead point when the configuration described in (v) occurs. In such situations, the mechanism cannot be operated by actuators since the actuators cannot provide forces along a direction parallel to the y-axis with all the mechanism's nodes located on the x-axis. Moreover, an external force parallel to the y-axis is needed to put the mechanism to use in its normal state. Furthermore, this characteristic brings an advantage to the mechanism. The mechanism can be folded in a small volume for transportation purposes.

5. Workspace

The actuator workspace of a mechanism is defined as the region that the actuators can operate while the output workspace is defined as the region that the end-effectors can reach. The boundaries and singular curves of a workspace usually correspond to the mechanism's singular configurations since, in such situations, the mechanism cannot be controlled or cannot generate certain displaces of its actuators and end-effectors.

5.1. Actuator Workspace. For the 4-bar tensegrity mechanism researched here, the actuator workspace consists of the ranges of variables, ρ_1 and ρ_2. Generally, the boundary of the actuator workspace and singular curves inside the actuator workspace always correspond to the singular configurations. Moreover, by plotting the curves of singular configurations described in Section 4.2, the actuator workspace of the mechanism can be obtained as shown in Figure 2.

From Figure 2, it can be seen that each curve is identified according to the singular configurations listed in Section 4.2. In addition, the singular configuration described in (v) corresponds to a point ($\rho_1 = \rho_2 = 20$ m) of the actuator workspace boundary. Moreover, the configuration described in (vi) corresponds to a singular point ($\rho_1 = \rho_2 = 10$ m) inside the actuator workspace.

Figure 2: Actuator workspace and singular curves for the planar 4-bar tensegrity mechanism with $L = 10$ m.

5.2. Output Workspace. The output workspace corresponds to the ranges of Cartesian coordinates of node F. In most cases, the output workspace can be obtained by mapping the actuator workspace into the output domain. However, the boundaries of the actuator workspace are not always corresponding to the boundaries of the output workspace. Generally, the output workspace can be obtained by analyzing the singular configurations and the corresponding behaviors of the mechanism. An example of the mechanism's output workspace and singular curves is shown in Figure 3.

From Figure 3, it can be seen that curve i corresponds to the singular configuration (i) described in Section 4.2. In addition, curve i takes the form

$$x^2 + y^2 = L^2. \tag{41}$$

Furthermore, curve iii corresponding to the singular configuration (iii) can be described by

$$(x - 2L)^2 + y^2 = L^2. \tag{42}$$

From Section 4.2, we know that the mechanism becomes uncontrollable when the singular configuration (vi) occurred. The node C is coincident with node D while node E is coincident with node F. Moreover, the force in the spring joining nodes E and F is equal to zero. The only possible deformation of the mechanism is a rotation with respect to node C of the strut joining nodes C and F. Therefore, the expression for the singular configuration (vi) in the output workspace can be written as

$$(x - x_c)^2 + (y - y_c)^2 = L^2, \tag{43}$$

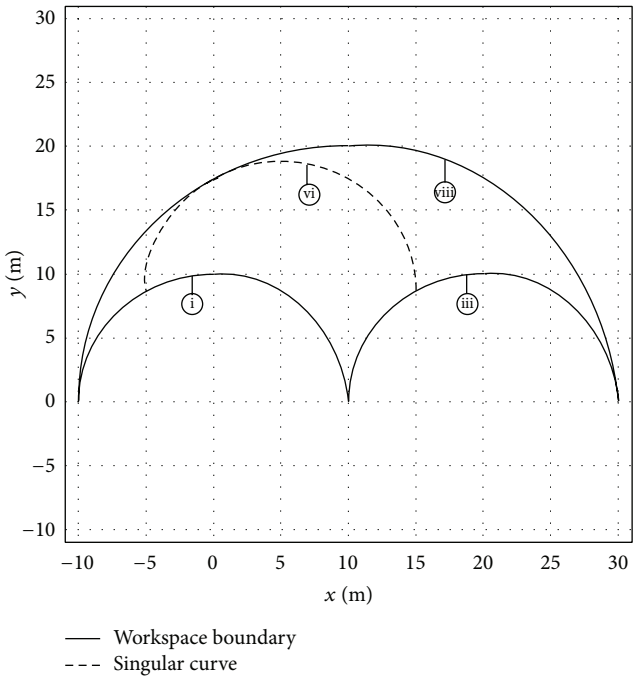

Figure 3: Output workspace and singular curves for the planar 4-bar tensegrity mechanism with $L = 10$ m.

where

$$x_c = \frac{L}{2}, \qquad y_c = \frac{\sqrt{3}L}{2}. \tag{44}$$

In (43), x_c and y_c are the Cartesian coordinates of node C with $\rho_1 = \rho_2 = L$.

From Figure 3, it can be observed that the curve viii does not correspond to any singular configuration described in Section 4.2. Moreover, curve viii is obtained by analyzing the behaviors of the mechanism. As illustrated in Figure 1, the movement of node C is a rotation with respect to node B while the movement of node F is a rotation with respect to node C. Therefore, when the node F generates a rotation centered on node B with $2L$ in radius, the end-effector of the mechanism, node F, will reach the boundaries of output workspace. Furthermore, the curve viii can be described by

$$(x - L)^2 + y^2 = (2L)^2. \tag{45}$$

Finally, the actuator workspace and output workspace are both obtained by analyzing the singular configurations and corresponding behaviors of the mechanism. The actuator and output workspaces of the planar tensegrity mechanism should be considered when such a mechanism is put to use or being designed.

6. Conclusion

Compared with conventional mechanisms, tensegrity mechanisms can be modeled with greater accuracy since all of their components are axially loaded. Furthermore, the use of springs in tensegrity allows them to have the advantage of being deployable. For this reason, tensegrity mechanisms can be viewed as one alternative solution to conventional mechanisms in some applications. In this paper, the kinematics, singularity, and workspaces of a planar 4-bar tensegrity mechanism were presented.

The analytical solutions to the forward and inverse kinematic problems were found by using an energy based method. Unlike conventional mechanisms, the shape of the 4-bar tensegrity mechanism depends not only on its geometry but also on the internal forces in the springs. As a consequence, the kinematic analysis should consider the constraint that the potential energy of the mechanism will reach its minimum when the mechanism is in equilibrium. Afterwards, a Jacobian was developed and the singular configurations were discussed. It was demonstrated that the finite movements of the actuators can be generated when the end-effector reached the boundaries of the output workspace. Moreover, the external loads exerted on the end-effector cannot be resisted by the actuators when the singular configurations corresponding to the singular curves inside the actuator workspace occurred. Furthermore, an attractive characteristic was found; that is, the mechanism can be folded in a small volume for transportation purposes. Finally, according to the singular configurations and the corresponding behaviors of the mechanism, the actuator and output workspaces were mapped. The singular configurations and workspaces of the mechanism should be considered when such a mechanism is put to use or being designed.

In future work, the authors wish to research the control of the 4-bar tensegrity mechanism.

Appendices

A. Details of Variables N_0, N_1, and E_ξ

Consider the following

$$\begin{aligned}
N_0 &= \frac{\rho_1^2 + \rho_2^2}{2L^2} - 1, \\
N_1 &= \frac{\rho_2\sqrt{4L^2 - \rho_2^2} - \rho_1\sqrt{4L^2 - \rho_1^2}}{2L^2}, \\
E_1 &= \frac{2\left(N_0^2 - N_1^2\right) - 2N_0\left(N_0^2 + N_1^2\right)}{N_1\left(N_0^2 + N_1^2\right) + 3N_0N_1}, \\
E_2 &= \frac{2N_0N_1}{N_1\left(N_0^2 + N_1^2\right) + 3N_0N_1}, \\
E_3 &= -\frac{2N_0\left(N_0^2 + N_1^2\right) + 2\left(N_0^2 - N_1^2\right)}{N_1\left(N_0^2 + N_1^2\right) + 3N_0N_1}, \\
E_4 &= -\frac{N_1\left(N_0^2 + N_1^2\right) + N_0N_1}{N_1\left(N_0^2 + N_1^2\right) + 3N_0N_1},
\end{aligned} \tag{A.1}$$

$$E_5 = \frac{E_2}{3} + \left[\frac{-q}{2} + \sqrt{\frac{q^2}{4} - \frac{p^3}{27}}\right]^{1/3} + \left[\frac{-q}{2} - \sqrt{\frac{q^2}{4} - \frac{p^3}{27}}\right]^{1/3}. \tag{A.2}$$

In (A.2), the expressions for p and q are as follows:

$$p = \left[E_1E_3 - 4E_4\right] - \frac{E_2^2}{3},$$
$$q = \frac{2}{27}E_2^3 + \frac{E_2}{3}\left[E_1E_3 - 4E_4\right] + \left[4E_2E_4 - E_1^2E_4 - E_3^2\right]. \tag{A.3}$$

B. Details of Variables λ_ζ

Consider the following

$$\lambda_1 = \frac{5}{L^2}\left[2Ly - G_0 - G_1L^2\right] - \frac{\rho_1^2 + 2L^2}{2L^2}G_2 + \frac{3G_3}{2},$$
$$\lambda_2 = \frac{1}{L^2}\left\{3\left[2x - \frac{\rho_1^2}{L}\right] + 2G_0\left[G_1 - \frac{2Ly - G_0}{L^2}\right] + \frac{1}{2}\left[2L^2 + \rho_1^2 - G_0\right]G_4 + 4\right\},$$
$$\lambda_3 = \frac{(2Ly - G_0)\left[2L^2 - 3\left(2Lx - \rho_1^2\right)\right]}{2L^4} - 2G_1\left(9 - \frac{\rho_1^2}{L^2}\right),$$
$$\lambda_4 = \frac{1}{L^2}\left\{3\left(2Lx - \rho_1^2\right) - 2L^2 - 2\left(2L^2 - \rho_1^2\right)\left(2Lx - \rho_1^2\right) + G_0G_1 + \left[G_0 - 2L^2 + \rho_1^2\right]G_4\right\},$$
$$\lambda_5 = \frac{3L^2 - 2\rho_1^2}{L^2} + \left(1 - \frac{\rho_1^2}{2L^2}\right)G_2 - \frac{1}{2}G_3. \tag{B.1}$$

In (B.1), the expressions for G_0–G_4 are as follows:

$$G_1 = \rho_1\sqrt{4L^2 - \rho_1^2},$$
$$G_2 = \frac{1}{2L^3}\left\{\rho_1\left[(x - L)\sqrt{4L^2 - \rho_1^2} - \rho_1y\right] + 2\rho_1^2y\right\},$$
$$G_3 = \frac{1}{4L^6}\left\{\rho_1\sqrt{4L^2 - \rho_1^2}\left[\left(2Lx - \rho_1^2\right)^2 - L^4\right] + \left(2L^2 - \rho_1^2\right) \times \left(2Ly - \rho_1\sqrt{4L^2 - \rho_1^2}\right)\left(2Lx - \rho_1^2\right)\right\},$$
$$G_4 = \frac{1}{2L^2}\left(2Ly - \rho_1\sqrt{4L^2 - \rho_1^2}\right)\left(2Lx - \rho_1^2\right),$$
$$G_5 = \frac{1}{2L^4}\left[\left(2Lx - \rho_1^2\right)^2 - 2L^4\right]. \tag{B.2}$$

Conflict of Interests

The authors declare that there is no conflict of interests regarding the publication of this paper.

Acknowledgment

This research is supported by the National Natural Science Foundation of China (no. 51375360) and the Fundamental Research Funds for the Central Universities (no. K505131000087).

References

[1] B. Fuller, "Tensile-integrity Structures," USA Patent 30,635,21, November 1965.

[2] K. Snelson, "Continuous Tension, Discontinuous Compression Structures," USA Patent 31,696,11, February 1965.

[3] R. Motro, "Tensegrity systems: the state of the art," *International Journal of Space Structures*, vol. 7, pp. 75–83, 1992.

[4] R. E. Skelton and M. C. Oliveira, *Tensegrity Systems*, Springer, New York, NY, USA, 2009.

[5] A. G. Tibert and S. Pellegrino, "Review of form-finding methods for tensegrity structures," *International Journal of Space Structures*, vol. 18, no. 4, pp. 209–223, 2003.

[6] K. Koohestani, "Form-finding of tensegrity structures via genetic algorithm," *International Journal of Solids and Structures*, vol. 49, no. 5, pp. 739–747, 2012.

[7] H. C. Tran and J. Lee, "Form-finding of tensegrity structures using double singular value decomposition," *Engineering with Computers*, vol. 29, pp. 71–86, 2013.

[8] N. Ben Kahla and K. Kebiche, "Nonlinear elastoplastic analysis of tensegrity systems," *Engineering Structures*, vol. 22, no. 11, pp. 1552–1566, 2000.

[9] A. Nuhoglu and K. A. Korkmaz, "A practical approach for nonlinear analysis of tensegrity systems," *Engineering with Computers*, vol. 27, no. 4, pp. 337–345, 2011.

[10] S. H. Juan and J. M. Mirats Tur, "Tensegrity frameworks: static analysis review," *Mechanism and Machine Theory*, vol. 43, no. 7, pp. 859–881, 2008.

[11] I. J. Oppenheim and W. O. Williams, "Tensegrity prisms as adaptive structures," in *in Proceedings of the ASME International Mechanical Engineering Congress and Exposition*, pp. 113–120, 1997.

[12] J. B. Bayat, *Position analysis of planar tensegrity structures [Ph.D. thesis]*, University of Florida, Gainesville, Fla, USA, 2006.

[13] M. Arsenault and C. M. Gosselin, "Kinematic and static analysis of a 3-PUPS spatial tensegrity mechanism," *Mechanism and Machine Theory*, vol. 44, no. 1, pp. 162–179, 2009.

[14] T. M. Tran, *Reverse displacement analysis for tensegrity structures [M.S. thesis]*, University of Florida, Gainesville, Fla, USA, 2002.

[15] M. Q. Marshall, *Analysis of tensegrity-based parallel platform devices [M.S. thesis]*, University of Florida, Gainesville, Fla, USA, 2003.

[16] M. Arsenault, "Stiffness analysis of a 2dof planar tensegrity mechanism," *Journal of Mechanisms and Robotics*, vol. 3, no. 2, Article ID 021011, 2011.

[17] S. Chen and M. Arsenault, "Workspace computation and analysis of a planar 2-DOF translational tensegrity mechanism," in *Proceedings of the ASME International Design Engineering*

Technical Conferences and Computers and Information in Engineering Conference (IDETC/CIE '10), pp. 223–232, August 2010.

[18] C. Sultan, M. Corless, and R. E. Skelton, "Tensegrity flight simulator," *Journal of Guidance, Control, and Dynamics*, vol. 23, no. 6, pp. 1055–1064, 2000.

[19] C. Sultan, M. Corless, and R. E. Skelton, "Peak to peak control of an adaptive tensegrity space telescope," in *Smart Structures and Materials, Mathematics and Control in Smart Structures*, Proceedings of SPIE, pp. 190–201, March 1999.

[20] C. Paul, F. J. Valero-Cuevas, and H. Lipson, "Design and control of tensegrity robots for locomotion," *IEEE Transactions on Robotics*, vol. 22, no. 5, pp. 944–957, 2006.

[21] C. Sultan and R. Skelton, "A force and torque tensegrity sensor," *Sensors and Actuators A: Physical*, vol. 112, no. 2-3, pp. 220–231, 2004.

[22] J. M. Mirats Tur and S. H. Juan, "Tensegrity frameworks: dynamic analysis review and open problems," *Mechanism and Machine Theory*, vol. 44, no. 1, pp. 1–18, 2009.

[23] M. Arsenault and C. M. Gosselin, "Static balancing of tensegrity mechanisms," *Journal of Mechanical Design*, vol. 129, no. 3, pp. 295–300, 2007.

[24] C. M. Gosselin, "Static balancing of spherical 3-DoF parallel mechanisms and manipulators," *International Journal of Robotics Research*, vol. 18, no. 8, pp. 819–829, 1999.

[25] S. M. M. Shekarforoush, M. Eghtesad, and M. Farid, "Design of statically balanced six-Degree-of-Freedom parallel mechanisms based on tensegrity system," in *Proceedings of the ASME International Mechanical Engineering Congress and Exposition (IMECE '09)*, pp. 245–253, November 2009.